ISTITUTO NAZIONALE DI RICERCA METROLOGICA
Repository Istituzionale

Non-self-similar light transport in scattering media

(Article begins on next page)

29 August 2024

Non-self-similar light transport in scattering media

Ernesto Pini [1,2] Giacomo Mazzamuto [1,2,3] Francesco Riboli [2,3] Diederik S. Wiersma [1,2,4] and Lorenzo Pattelli [2,3,4,*]

[1]*Department of Physics and Astronomy, Università di Firenze, Sesto Fiorentino 50019, Italy*
[2]*European Laboratory for Non-linear Spectroscopy (LENS), Sesto Fiorentino 50019, Italy*
[3]*National Research Council – National Institute of Optics (CNR-INO), Sesto Fiorentino 50019, Italy*
[4]*Istituto Nazionale di Ricerca Metrologica (INRiM), Turin 10135, Italy*

Transport processes underpin a wide variety of phenomena, ranging from chemistry, to physics and ecology. Despite their pervasiveness, however, several distinctive features of these processes are still elusive, making it difficult to recognize and classify the associated transport regimes. Using light scattering as a probe to explore different propagation regimes, we report on the experimental observation of non-self-similar light transport through turbid membranes. Our results show that a breakdown of self-similarity can arise for light waves even in the presence of isotropic and homogeneous disorder, and can be tuned by varying the turbidity of the system. By introducing the concept of self-similarity for light propagation, we provide a unified framework for the classification of light transport regimes—overcoming the dichotomy between normal and anomalous diffusion—and show that non-self-similar propagation is a common and experimentally accessible phenomenon. This insight can help to understand and model other scenarios where light transport is dominated by rare propagation events, such as in nonlinear and active media, but also in other fields of research beyond optics.

Introduction. Light transport experiments are traditionally a fertile playground for the study of novel transport regimes, often allowing to cast intriguing parallels between the propagation dynamics in seemingly unrelated research fields [1]. In most cases, however, peculiar structural and/or optical properties must be purposely introduced in a scattering material in order to observe anomalous diffusion, such as tailored spatial correlations [2–11] or wavefront-shaped illumination conditions [12–14]. For instance, transient anomalous transport regimes were previously observed in structures with carefully engineered fractal heterogeneous inclusions [15–18]. Conversely, more trivial propagation dynamics is typically expected when dealing with simpler disorder realizations and illumination schemes.

One of the simplest configurations that can be considered for a scattering medium is that of a plane-parallel slab, a prototypical model that is commonly used as a basic geometry for the study of radiative transport problems. In many of such cases, the coherent aspects of light propagation can be disregarded (e.g., by performing dynamic or ensemble averaging over different realizations of disorder), and an exact solution can be found using standard results from scalar radiative transfer theory or Monte Carlo (MC) simulations. These solutions are typically assumed to be devoid of peculiar features, as

radiative transfer theory requires that scattering centers are placed at statistically independent positions, and in the far field of one another [19,20].

As a result, the optical properties of a scattering slab configuration are largely determined by the simple ratio between the physical thickness of the slab and its transport mean free path, also known as the optical thickness L/l_t. When decreasing the optical thickness (e.g., by diluting the density of scattering centers), the onset of a multiple scattering process in the slab plane is often neglected altogether, as most of the light impinging on the slab will pass through it in a ballistic fashion. Even in optically thin samples, however, a small fraction of light will still propagate over large distances through multiple scattering events, owing to the unbound lateral extent of the plane-parallel slab geometry [21–23]. This results in a peculiar radiative transport regime which should still fall under the validity assumptions of radiative transfer theory, and yet remained largely unexplored.

In this Letter, we investigate this elusive regime experimentally by reconstructing the moment scaling spectrum of the intensity profiles transmitted through thin scattering films, revealing the hallmarks of a generalized transport anomaly related to the degree of self-similarity of the transient spatial profiles. The onset of this anomalous regime is associated with an enhancement of the in-plane propagation rate which persists at late times, despite the isotropic, dilute, and statistically independent positions of scattering centers in the disordered slab. Traditionally, the classification of anomalous transport regimes is based on the power-law scaling of their associated mean-squared displacement or variance $\langle x^2 \rangle$: We call "normal" a transport process whose spatial variance grows linearly with time, and "anomalous" everything else [24]. This
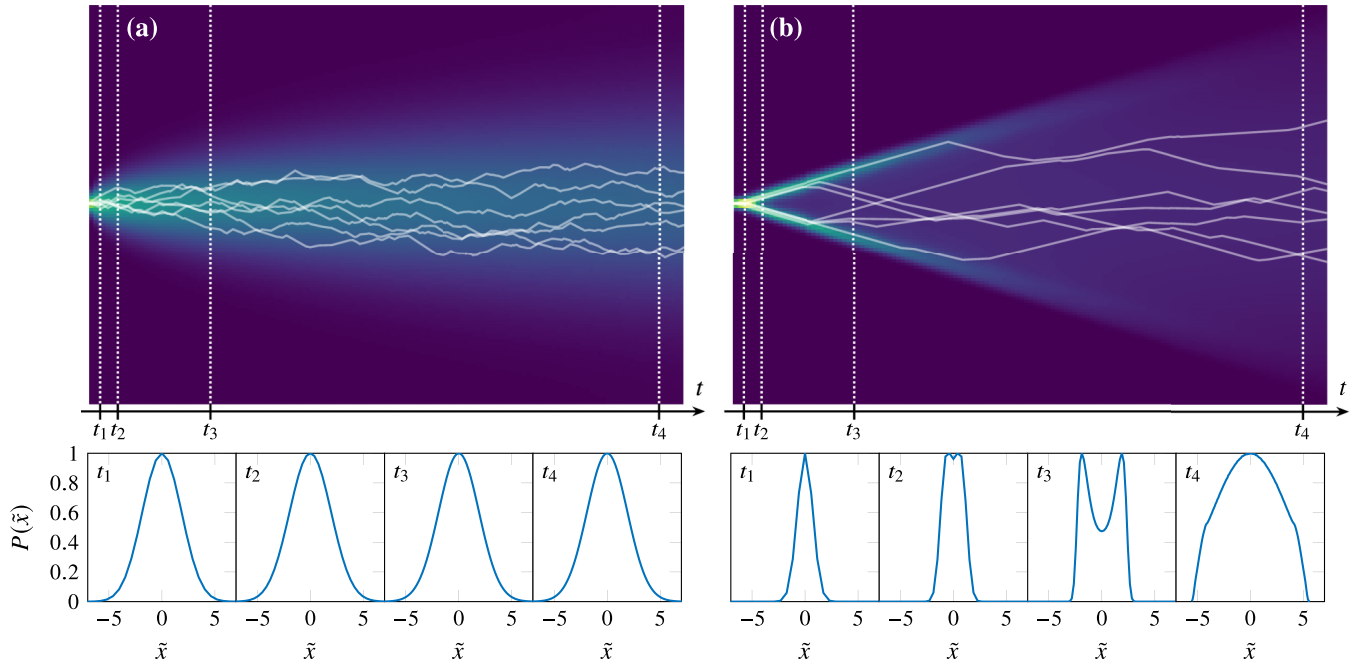
FIG. 1. Probability density distributions for a numerical unidimensional propagation example. A few space-time trajectories are superimposed for illustrative purposes. Crosscuts of the normalized distributions at different delays are shown in the lower panels. (a) In the case of strongly self-similar processes, the normalized spatial profiles can be rescaled ($xt^{-1/\nu} \to \tilde{x}$) onto a single profile $P(\tilde{x})$ at all times, due to the fact that all spatial moments follow the same q/ν scaling law. (b) For more general non-self-similar processes, no simple rescaling operation can be applied.

classification scheme has obvious limitations, as it is unable to distinguish the onset of different propagation regimes [25], and can easily misclassify highly anomalous systems as simple examples of normal diffusion. For this purpose, we can apply a richer description based on the scaling behavior of all moments $\langle |x|^q \rangle \propto t^{\gamma_q}$, rather than just the variance [26]. Studying the power-law growth of different moments of displacement enables a more correct and general classification of all possible transport regimes. This can be done by building the full moment scaling spectrum of the process, which is obtained by considering the power-law exponents γ_q associated with different qth moments, and evaluating the self-similarity of their collective scaling [26–28]. In this framework, a transport process is termed strongly self-similar if all moments follow the same scaling law $\gamma_q = q/\nu$ for some constant ν (hence γ_q grows linearly). Two simple cases exhibiting strong self-similarity are ballistic propagation and normal diffusion, for which $\nu = 1$ and $\nu = 2$, respectively. Superdiffusion is also a typical strongly self-similar regime, characterized by a constant value $1 < \nu < 2$. Alternatively, transport can be weakly self-similar: In this case the moment scaling spectrum is divided in two self-similar regions characterized by different ν values. This typically happens when the tails of the distribution scale at a faster rate than the core, leading to a piecewise-linear moment scaling spectrum. In principle, however, one could envision a more general situation where each moment follows a different scaling law. In this case, which we dub *non-self-similar*, γ_q can be a more complex function of q, and self-similarity is lost altogether.

A qualitative depiction of the typical hallmarks of self-similar versus non-self-similar transport is shown in Fig. 1

for an illustrative unidimensional case. In the strongly self-similar case, the probability density functions $P(x, t)$ can be collapsed onto a single functional shape $F(\tilde{x})$ using a rescaling operation mapping $xt^{-1/\nu} \to \tilde{x}$. In the non-self-similar case this is not possible, as can be seen intuitively by the fact that the spatial profiles have altogether different shapes at different times. Based on this framework, self-similarity has been explored numerically for a variety of synthetic stochastic models [28–34], but experimental studies in this field are still scarce [35–37] due to the lack of a flexible platform where the properties of these transport phenomena can be consistently observed and tuned. Moreover, most models and systems studied to date exhibit only a weak self-similarity resulting from the superposition of two separate self-similar processes have been reported, rather than a full breakdown of self-similarity distributed along the whole moment scaling spectrum. This raises the question as to what extent can transport processes actually deviate from self-similarity.

Results and discussion. We address this question by exploring self-similarity experimentally in the case of light transport. To this purpose, we prepare samples with different scatterer densities and use a transient-imaging apparatus capable of recording the spatial and temporal evolution of the transmitted intensity profiles based on an optical gating scheme [38]. In the experiment, the time-resolved transmittance of a 150 fs probe pulse through the scattering sample is sampled via nonlinear sum-frequency generation with a collimated gate pulse impinging on a nonlinear crystal, at a repetition rate of 80 MHz. The probe and gate beam wavelengths are 1525 and 820 nm, respectively. A CCD camera collects the transmitted profiles at different delays, from which the spatial
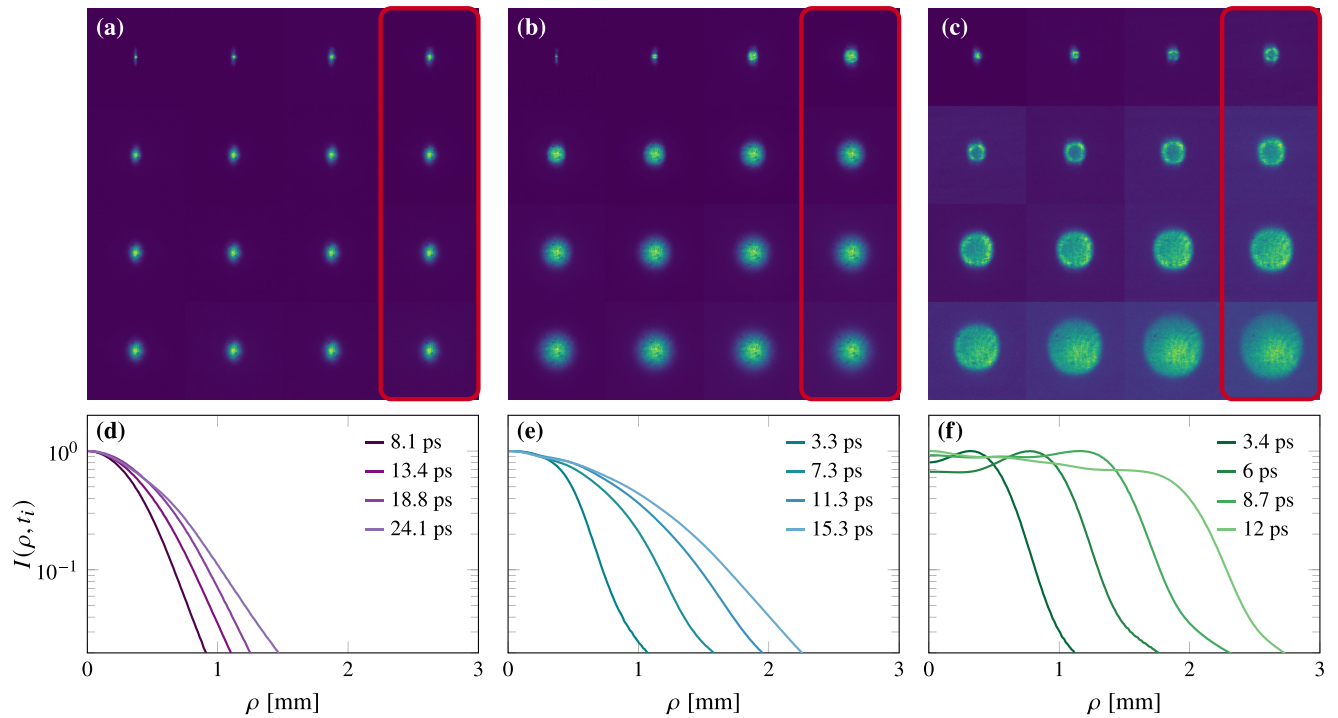
FIG. 2. (a)–(c) Transmitted profiles recorded at different times t_i for three 100-μm-thick samples with different turbidity (samples A, B, and C in order of decreasing turbidity from left to right). Each frame covers the same area of $7.4 \times 7.4 \, \text{mm}^2$ and is normalized to its maximum value. Time delays between consecutive frames are $\Delta t = 1.33$, 1.0, and 0.67 ps, respectively, for the three cases. (d)–(f) Representative radially averaged profiles corresponding to the highlighted frames. A time-evolving intensity profile is visible for the least scattering sample C: The spatial distribution of light evolves from a ring-shaped profile towards a top-hat-like distribution, showing one of the typical hallmarks of non-self-similarity.

moments can be directly calculated. The integration time of each frame varies between 1 and 2500 s, depending on the decreasing intensity available at increasing time delays. The experimental samples consist of free-standing scattering films made of a dilute dispersion of TiO_2 nanoparticles in a UV-cured transparent polymer matrix (see the Appendix). Three samples with the same thickness ($L = 100 \pm 1 \, \text{μm}$) and different particle densities have been prepared, up to a maximum volume fraction of about 3%.

For each sample—referred to as samples A, B, and C in order of decreasing turbidity—multiple transmitted intensity measurements were recorded and averaged over different positions to obtain the incoherent transmitted intensity profiles at different times t_i [Figs. 2(a)–2(c)]. Due to the isotropic structure of the scattering samples, a radial average around the illumination axis can be performed to obtain the profiles $I(\rho, t_i)$ [Figs. 2(d)–2(f)]. Notably, the profile shape of the instantaneous spatial intensity distributions is independent of the presence of spurious absorption or intensity drifts of the laser sources, which could only result in a modulation of their amplitude, hence leaving the spectrum of their spatial moments unaffected. For the same reason, the spatial moments of transmittance profiles recorded using different integration times can also be directly compared without any further normalization.

The asymptotic growth rate of the second moment (variance) of the transmittance profiles is typically considered as a direct measurement of the diffusion rate in a scattering

system [38,39]. We use this observable to retrieve the effective transport mean free path of the considered samples by finding the best-fit Monte Carlo (MC) simulation [40] to the experimental data for each sample [Fig. 3(a)]. Simulations are performed setting an effective refractive index n estimated using the Maxwell-Garnett formula based on the different TiO_2/resin volume ratios, and an asymmetry factor $g = 0.16$ given by Mie theory for the average experimental particle size of 280 nm at the probe wavelength of 1525 nm. However, the exact value of g does not influence the results significantly, as expected for transport in the multiple scattering regime. The analysis returned l_t values of 53 ± 4, 195 ± 11, and $630 \pm 30 \, \text{μm}$ for samples A, B, and C, respectively, corresponding to optical thicknesses of 1.9 ± 0.3, 0.51 ± 0.05, and 0.158 ± 0.017.

The experimental measurements reveal that the observed asymptotic transverse propagation rate for these samples is much larger than that expected from the l_t values retrieved by MC fitting. In other words, even after several scattering events, the transverse intensity profiles expand far more quickly than what could be expected based on the nominal transport mean free path, reaching values of the mean-squared displacement growth rate for the samples A, B, and C of $1.687 \times 10^4 \, \text{m}^2 \, \text{s}^{-1}$, $7.624 \times 10^4 \, \text{m}^2 \, \text{s}^{-1}$, and $2.714 \times 10^5 \, \text{m}^2 \, \text{s}^{-1}$, respectively.

The agreement found between experimental results and Monte Carlo simulations suggests an interpretation for the observed enhancement of the mean-square displacement growth
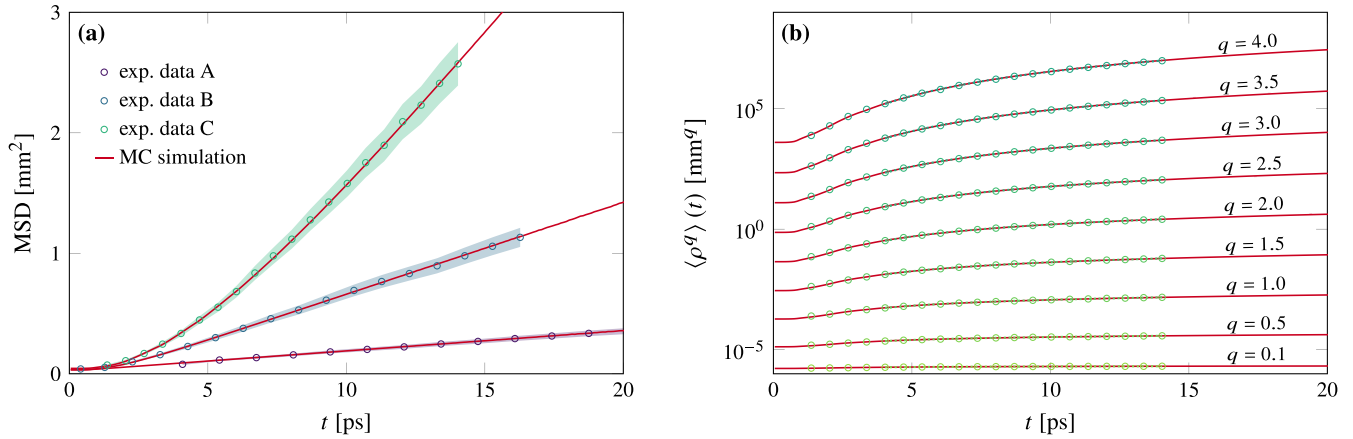
FIG. 3. (a) Temporal evolution of the experimental mean-squared displacement (MSD). Fitting each curve with a corresponding MC simulation returns their associated transport mean free path values. Shaded areas represent 1σ confidence intervals. (b) Temporal evolution of a subset of the moments of displacement ($0.1 \leqslant q \leqslant 4$) for sample C, fitted with Eq. (2) for $t > l_t n/c$ (dotted) to retrieve γ_q. The output of the corresponding MC simulations is also shown (solid, red).

rate in terms of the occurrence of exceedingly long steps in long-lived trajectories. In other words, with decreasing optical thickness, light spending a longer time inside the sample undergoes fewer scattering events than what should be expected based on the particle density in the sample, showing a sort of "survival bias" for light [22]. The dynamic modification of the effective path length distribution followed by the subset of survived trajectories is such to break transport self-similarity in these samples, giving rise to a different type of propagation which remains fully compatible with the validity assumptions of the radiative transfer equation (especially so for the most diluted sample C), as confirmed by the excellent agreement with MC simulations.

A more quantitative analysis of this phenomenon can be performed by considering the spectrum of all qth moments at different times, defined as

$$\langle \rho^q \rangle(t) = \frac{\int_0^\infty \rho^q I(\rho, t)\rho \, d\rho}{\int_0^\infty I(\rho, t)\rho \, d\rho} \qquad (1)$$

for a generic intensity distribution $I(\rho, t)$, with q in the positive real numbers. The growth rate of each moment can be fitted using a power-law model

$$\langle \rho^q \rangle(t) \sim (t - t_q)^{\gamma_q}, \qquad (2)$$

where γ_q is the exponent associated with the qth moment and t_q is temporal offset which can be introduced to exclude the early transient and small up-conversion artifacts associated with the tight ballistic laser spot.

The moment growth rates were fitted with Eq. (2) in a time range following the early quasiballistic transient ($t > l_t n/c$). The resulting moment scaling spectra are shown in Fig. 4(a), together with the corresponding results obtained for MC simulations performed with the previously determined l_t values. The varying degree of self-similarity exhibited by the three different samples is highlighted in Fig. 4(b), where the moment scaling spectrum is plotted normalized to the strongly self-similar diffusive case $\gamma(q) = q/2$. At an optical thickness of 1.9, sample A shows a moment scaling spectrum which is fully consistent with a strongly self-similar transport regime,

exhibiting the same power-law scaling of normal diffusion. On the other hand, samples B and C exhibit hallmarks of both anomalous (superdiffusive) and non-self-similar transport.

Due to the finite size of physical samples, real step length distributions cannot exhibit diverging moments, and different
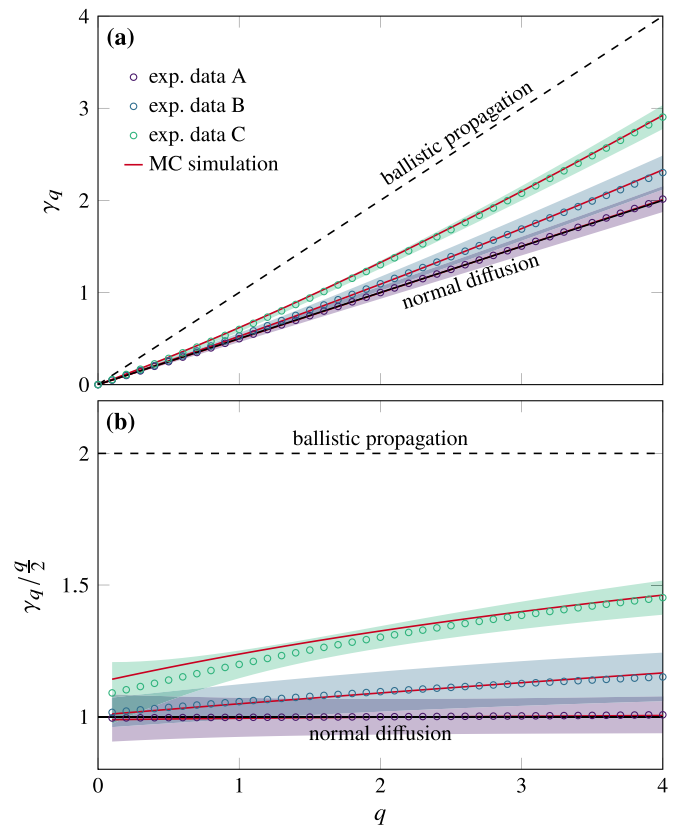

FIG. 4. (a) Experimental and simulated moment scaling spectra, and (b) same curves normalized to strong self-similar normal diffusion. The solid and dashed black lines represent the case of strong self-similar normal diffusion and ballistic transport, respectively. Shaded areas in both graphs represent 1σ confidence intervals
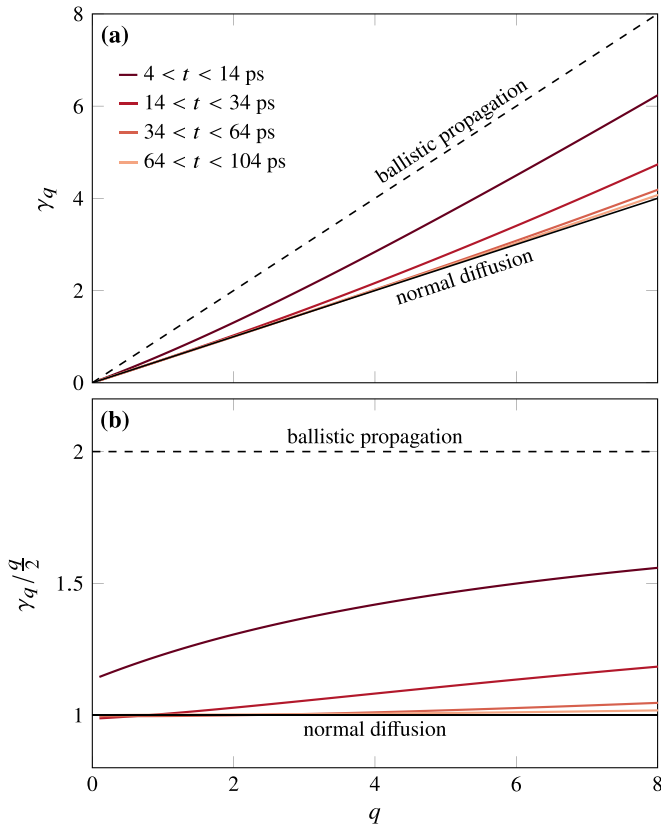
FIG. 5. (a) Moment scaling spectra for sample C calculated for nonoverlapping fitting time intervals at increasing delays, and (b) same curves normalized to strong self-similar normal diffusion. The solid and dashed black lines represent the case of strong self-similar transport, respectively, for normal diffusion and ballistic transport.

transport regimes are necessarily expected to onset at different timescales after the initial anomalous stage. To this purpose, we rely on numerical calculations with large statistics (10^{12} trajectories) to study how the observed transport regime evolves asymptotically for $t \to \infty$ in the case of the least scattering configuration (sample C). Building the moment scaling spectrum for $0.1 < q < 8$ for increasingly delayed time ranges shows that the transmitted intensity profiles evolve from a superdiffusive and non-self-similar behavior, to a moment spectrum compatible with strongly self-similar normal diffusion (see Fig. 5). For the sample with a nominal optical thickness of 0.158, this transition to the strongly self-similar regime eventually occurs at a delay >60 ps, corresponding to a total path length of >1 cm, well within the multiple scattering regime ($\approx 20\,l_t$). On the other hand, the in-plane diffusion rate enhancement with respect to the nominal transport mean free path persists also in the limit for $t \to \infty$, i.e., even after the transport regime has converged to its asymptotic and strongly self-similar final form, confirming that the step length distribution effectively sampled by light traveling inside optically thin membranes features fat tails favoring steps longer than expected for the given particle density.

Conclusions. We studied the propagation of light in optically thin media with homogeneous disorder, performing a full moment scaling spectrum analysis that revealed the presence of anomalous transport transient regimes which can be superdiffusive and non-self-similar.

The application of this type of analysis is still sporadic in the literature [25,41], despite its unique ability to identify different transport regimes and highlight otherwise hidden properties. For example, the observation of weakly self-similar mobility of polymer particles unveiled the presence of active transport mechanisms inside living cancer cells [36,42], or the occurrence of bulk-mediated long jumps for particles being adsorbed and desorbed on planar lipid bilayers [37]. Similarly, non-self-similarity in the dispersion dynamics of Arctic sea ice hints at the occurrence of fracturing and faulting events [35], even though correcting for the mean drift flow remains challenging [43].

In this Letter we have shown that light can exhibit a general and tunable breakdown of self-similarity, which changes continuously along its moment spectrum and can be studied under experimentally controlled conditions. Scattering membranes with a low optical thickness, therefore, provide an ideal system for studying this fascinating physics which includes non-Gaussian diffusion [41], extreme events [44], transient return probabilities [45], or visitation statistics [46], to name a few.

Other relevant examples of transient light transport regimes exhibiting an enhanced or suppressed propagation rate are known in the literature, such as those associated with Lévy glasses [2,17,47], or spatially quenched scatterer distributions [15,18,48]. It should be stressed, however, that the peculiar transport regime observed in this work is of a fundamentally different type compared to these previous cases. Indeed, the samples that we have studied exhibit the simplest type of random and uncorrelated disorder typical of dilute nanoparticle mixtures. Moreover, the effect that we observe persists even when averaging over different disorder configurations, as confirmed both experimentally and by the agreement with annealed-disorder MC simulations.

The lack of self-similarity exhibited by light transport in thin scattering membranes is not associated with ballistic propagation in the slab plane nor with a particular type of scatterer or illumination condition, as confirmed by its persistence after multiple scattering events. As such, it could be relevant to study whether its associated transverse propagation enhancement has any impact on the well-known invariance property for the average path length in scattering media, which should in principle remain valid up to arbitrary precision also for optically thin samples [49]. Most importantly, this type of non-self-similar transport arises without the need to postulate the presence of specific conditions such as heterogeneous disorder, active transport mechanisms, or jumps mediated through different embedding media—which suggests that the occurrence of weakly or altogether non-self-similar transport transients in confined geometries may be far more frequent than currently assumed.

Titan X Pascal GPU used for this research. L.P. wishes to thank F. Martelli and S. Lepri for discussion. E.P. thanks S. Donato for his help with sample preparation. D.S.W. acknowledges financial support from the European Union's Horizon 2020 Research and Innovation Programme under FET-OPEN Grant Agreement No. 828946 (PATHOS).

Appendix: Sample fabrication. Three samples were fabricated with a thickness of $L = 100 \pm 1 \, \mu m$ and different scattering densities, targeting optical thickness values between 0.1 and 10, i.e., spanning across the ballistic-to-diffusive transition.

The samples are composed of a mixture of a transparent UV-curable resin (Norland Optical Adhesive 65) and titanium dioxide nanoparticles (Tioxide RX-L) with an average diameter of 280 nm. The refractive indices of the resin and the nanoparticles at $\lambda = 1525 \, nm$ are $n = 1.51$ and $n = 2.47$, respectively. Three mixtures with TiO_2/resin mass fractions of 0.1, 0.02, and 0.005 were prepared, as determined using a precision balance. Assuming spherical particles and a specific gravity of $3.55 \, g \, cm^{-3}$, these correspond to estimated particle volume fractions of 0.034, 0.0068, and 0.0017 for samples A, B and C, respectively.

The mixtures are magnetically stirred for at least 2 h, and then infiltrated by capillary action between two microscope slides with a controlled gap. The slides are coated by a thin film of water-soluble polyvinyl alcohol (PVA) to facilitate their subsequent removal after UV curing of the sample, and glued together using NIST glass microspheres with a diameter of 100 μm as calibrated spacers to control the thickness of the gap. The sample is exposed to a 35-W UV lamp for 6 h to cure the scattering mixture (the nominal curing time of the transparent resin is around 5 min, but the presence of TiO_2 nanoparticles slows down the curing process). Finally, the resulting cells are left in water to dissolve the PVA layers and allow the release of the sample as a free-standing film. The samples are then cured again under UV light for a few hours on each side to ensure their complete polymerization.

This process results in flexible, free-standing slabs with a central scattering region of at least 5 cm^2 where the transport measurements are performed. Besides the scattering area, two transparent regions are used to measure the exact sample thickness optically through time-of-flight measurement of internally reflected light, and to precisely determine the absolute origin of the time-domain axis.

---

[1] D. S. Wiersma, Disordered photonics, Nat. Photon. **7**, 188 (2013).

[2] J. Bertolotti, K. Vynck, L. Pattelli, P. Barthelemy, S. Lepri, and D. S. Wiersma, Engineering disorder in superdiffusive Lévy glasses, Adv. Funct. Mater. **20**, 965 (2010).

[3] L. Shi, Y. Zhang, B. Dong, T. Zhan, X. Liu, and J. Zi, Amorphous photonic crystals with only short-range order, Adv. Mater. **25**, 5314 (2013).

[4] L. S. Froufe-Pérez, M. Engel, J. J. Sáenz, and F. Scheffold, Band gap formation and Anderson localization in disordered photonic materials with structural correlations, Proc. Natl. Acad. Sci. USA **114**, 9570 (2017).

[5] L. D. Negro and S. Inampudi, Fractional transport of photons in deterministic aperiodic structures, Sci. Rep. **7**, 2259 (2017).

[6] S. R. Sellers, W. Man, S. Sahba, and M. Florescu, Local self-uniformity in photonic networks, Nat. Commun. **8**, 14439 (2017).

[7] S.-Y. Jeon, H. Kwon, and K. Hur, Intrinsic photonic wave localization in a three-dimensional icosahedral quasicrystal, Nat. Phys. **13**, 363 (2017).

[8] G. J. Aubry, L. S. Froufe-Pérez, U. Kuhl, O. Legrand, F. Scheffold, and F. Mortessagne, Experimental tuning of transport regimes in hyperuniform disordered photonic materials, Phys. Rev. Lett. **125**, 127402 (2020).

[9] A. Patsyk, U. Sivan, M. Segev, and M. A. Bandres, Observation of branched flow of light, Nature (London) **583**, 60 (2020).

[10] S. Yu, C.-W. Qiu, Y. Chong, S. Torquato, and N. Park, Engineered disorder in photonics, Nat. Rev. Mater. **6**, 226 (2021).

[11] K. Vynck, R. Pierrat, R. Carminati, L. S. Froufe-Pérez, F. Scheffold, R. Sapienza, S. Vignolini, and J. J. Sáenz, Light in correlated disordered media, Rev. Mod. Phys. **95**, 045003 (2023).

[12] S. Rotter and S. Gigan, Light fields in complex media: Mesoscopic scattering meets wave control, Rev. Mod. Phys. **89**, 015005 (2017).

[13] J. Böhm, A. Brandstötter, P. Ambichl, S. Rotter, and U. Kuhl, *In situ* realization of particlelike scattering states in a microwave cavity, Phys. Rev. A **97**, 021801(R) (2018).

[14] H. Yılmaz, C. W. Hsu, A. Yamilov, and H. Cao, Transverse localization of transmission eigenchannels, Nat. Photon. **13**, 352 (2019).

[15] P. Barthelemy, J. Bertolotti, K. Vynck, S. Lepri, and D. S. Wiersma, Role of quenching on superdiffusive transport in two-dimensional random media, Phys. Rev. E **82**, 011101 (2010).

[16] P. Buonsante, R. Burioni, and A. Vezzani, Transport and scaling in quenched two-and three-dimensional Lévy quasicrystals, Phys. Rev. E **84**, 021105 (2011).

[17] R. Savo, M. Burresi, T. Svensson, K. Vynck, and D. S. Wiersma, Walk dimension for light in complex disordered media, Phys. Rev. A **90**, 023839 (2014).

[18] T. Svensson, K. Vynck, E. Adolfsson, A. Farina, A. Pifferi, and D. S. Wiersma, Light diffusion in quenched disorder: Role of step correlations, Phys. Rev. E **89**, 022141 (2014).

[19] M. I. Mishchenko, L. D. Travis, and A. A. Lacis, *Multiple Scattering of Light by Particles: Radiative Transfer and Coherent Backscattering* (Cambridge University Press, Cambridge, UK, 2006).

[20] A. Doicu and M. I. Mishchenko, Overview of methods for deriving the radiative transfer theory from the Maxwell equations. I: Approach based on the far-field Foldy equations, J. Quant. Spectrosc. Radiat. Transfer **220**, 123 (2018).

[21] M. Leonetti and C. López, Measurement of transport mean-free path of light in thin systems, Opt. Lett. **36**, 2824 (2011).

[22] L. Pattelli, G. Mazzamuto, D. S. Wiersma, and C. Toninelli, Diffusive light transport in semitransparent media, Phys. Rev. A **94**, 043846 (2016).

[23] G. Mazzamuto, L. Pattelli, C. Toninelli, and D. Wiersma, Deducing effective light transport parameters in optically thin systems, New J. Phys. **18**, 023036 (2016).

[24] R. Metzler, J.-H. Jeon, A. G. Cherstvy, and E. Barkai, Anomalous diffusion models and their properties: non-stationarity, non-ergodicity, and ageing at the centenary of single particle tracking, Phys. Chem. Chem. Phys. **16**, 24128 (2014).

[25] G. Muñoz-Gil, G. Volpe, M. A. Garcia-March, E. Aghion, A. Argun, C. B. Hong, T. Bland, S. Bo, J. A. Conejero, N. Firbas *et al.*, Objective comparison of methods to decode anomalous diffusion, Nat. Commun. **12**, 6253 (2021).

[26] R. Ferrari, A. Manfroi, and W. Young, Strongly and weakly self-similar diffusion, Physica D **154**, 111 (2001).

[27] P. Castiglione, A. Mazzino, P. Muratore-Ginanneschi, and A. Vulpiani, On strong anomalous diffusion, Physica D **134**, 75 (1999).

[28] K. Andersen, P. Castiglione, A. Mazzino, and A. Vulpiani, Simple stochastic models showing strong anomalous diffusion, Eur. Phys. J. B **18**, 447 (2000).

[29] R. Artuso and G. Cristadoro, Anomalous transport: A deterministic approach, Phys. Rev. Lett. **90**, 244101 (2003).

[30] D. N. Armstead, B. R. Hunt, and E. Ott, Anomalous diffusion in infinite horizon billiards, Phys. Rev. E **67**, 021110 (2003).

[31] A. Rebenshtok, S. Denisov, P. Hänggi, and E. Barkai, Non-normalizable densities in strong anomalous diffusion: Beyond the central limit theorem, Phys. Rev. Lett. **112**, 110601 (2014).

[32] E. Aghion, D. A. Kessler, and E. Barkai, Large fluctuations for spatial diffusion of cold atoms, Phys. Rev. Lett. **118**, 260601 (2017).

[33] X. Wang, Y. Chen, and W. Deng, Strong anomalous diffusion in two-state process with Lévy walk and Brownian motion, Phys. Rev. Res. **2**, 013102 (2020).

[34] J. Vollmer, L. Rondoni, M. Tayyab, C. Giberti, and C. Mejía-Monasterio, Displacement autocorrelation functions for strong anomalous diffusion: A scaling form, universal behavior, and corrections to scaling, Phys. Rev. Res. **3**, 013067 (2021).

[35] P. Rampal, J. Weiss, D. Marsan, and M. Bourgoin, Arctic sea ice velocity field: General circulation and turbulent-like fluctuations, J. Geophys. Res. **114**, C10014 (2009).

[36] N. Gal and D. Weihs, Experimental evidence of strong anomalous diffusion in living cells, Phys. Rev. E **81**, 020903(R) (2010).

[37] D. Krapf, G. Campagnola, K. Nepal, and O. B. Peersen, Strange kinetics of bulk-mediated diffusion on lipid bilayers, Phys. Chem. Chem. Phys. **18**, 12633 (2016).

[38] L. Pattelli, R. Savo, M. Burresi, and D. S. Wiersma, Spatio-temporal visualization of light transport in complex photonic structures, Light: Sci. Appl. **5**, e16090 (2016).

[39] L. A. Cobus, G. Maret, and A. Aubry, Crossover from renormalized to conventional diffusion near the three-dimensional Anderson localization transition for light, Phys. Rev. B **106**, 014208 (2022).

[40] L. Pattelli and G. Mazzamuto, Experimental imaging and Monte Carlo modeling of ultrafast pulse propagation in thin scattering slabs, J Biomed. Opt. **27**, 083020 (2022).

[41] B. Wang, J. Kuo, S. C. Bae, and S. Granick, When Brownian diffusion is not Gaussian, Nat. Mater. **11**, 481 (2012).

[42] D. Goldstein, T. Elhanan, M. Aronovitch, and D. Weihs, Origin of active transport in breast-cancer cells, Soft Matter **9**, 7167 (2013).

[43] A. Gabrielski, G. Badin, and L. Kaleschke, Anomalous dispersion of sea ice in the Fram Strait region, J. Geophys. Res. **120**, 1809 (2015).

[44] A. Vezzani, E. Barkai, and R. Burioni, Rare events in generalized Lévy walks and the big jump principle, Sci. Rep. **10**, 2732 (2020).

[45] N. Levernier, O. Bénichou, and R. Voituriez, Universality classes of hitting probabilities of jump processes, Phys. Rev. Lett. **126**, 100602 (2021).

[46] L. Régnier, M. Dolgushev, S. Redner, and O. Bénichou, Universal exploration dynamics of random walks, Nat. Commun. **14**, 618 (2023).

[47] P. Barthelemy, J. Bertolotti, and D. S. Wiersma, A Lévy flight for light, Nature (London) **453**, 495 (2008).

[48] R. Burioni, L. Caniparoli, and A. Vezzani, Lévy walks and scaling in quenched disordered media, Phys. Rev. E **81**, 060101(R) (2010).

[49] F. Martelli, F. Tommasi, A. Sassaroli, L. Fini, and S. Cavalieri, Verification method of Monte Carlo codes for transport processes with arbitrary accuracy, Sci. Rep. **11**, 19486 (2021).